

Lab-on-CD microfluidic platform for rapid separation and mixing of plasma from whole blood

Ju-Nan Kuo · Bo-Shiun Li

Published online: 20 March 2014
© Springer Science+Business Media New York 2014

Abstract Traditional clinical methods for separating whole blood into blood cells and cell-free plasma are labor intensive and time consuming. Accordingly, the present study proposes a simple compact disk (CD) microfluidic platform for the rapid separation of plasma from whole human blood and the subsequent mixing of the plasma with a suitable reagent. The performance of three CD microfluidic platforms incorporating square-wave mixing channels with different widths is evaluated both numerically and experimentally. The results show that given an appropriate specification of the microchannel geometry and a CD rotation speed of 2000 rpm, a separation efficiency of 95 % can be achieved within 5~6 s given a diluted blood sample with a hematocrit concentration of 6 %. Moreover, a mixing efficiency of more than 96 % can be obtained within 5 s given a CD rotation speed of 2200 rpm. The practical feasibility of the proposed device is demonstrated by performing a prothrombin time (PT) test. It is shown that while the time required to perform the PT test using a conventional bench top system is around 15 min, the proposed CD microfluidic platform allows the test to be completed within 1 min.

Keywords Lab-on-CD · Microchannel · Microfluidic · Mixing · Plasma separation

1 Introduction

Blood tests are one of the most common types of medical diagnostic test. In general, whole human blood consists

predominantly of blood cells (e.g., erythrocytes (red blood cells, RBCs), leukocytes (white blood cells, WBCs), and thrombocytes (platelets)) and plasma. The red blood cells constitute about 45 % of the whole blood, while the white blood cells account for around 1 %. Finally, the plasma accounts for nearly 54 % of the total blood volume, and is a complex solution containing more than 90 % water. The major solute of plasma comprises a heterogeneous group of proteins, composed primarily of albumin, globulin and fibrinogen. In performing a blood test, the first step is generally to separate the blood plasma (or cell-free serum) from the whole human blood so as to avoid protein confounding effects by the red and white blood cells (Toner and Irimia 2005). However, standard clinical methods for separating cell-free plasma from whole blood are labor intensive and time-consuming. Furthermore, having separated the blood plasma, it must then be removed from the plasma/blood cell reservoir and transferred to another device to be mixed with a suitable reagent so as to facilitate quantitative blood assays, such as urea, creatinine and PT tests (Jackson and Esnouf 2005). In practice, the sequential single-batch plasma separation and analysis procedures can take up to several hours to complete, and require the intervention of qualified technical personnel. Consequently, they are generally confined to professional, well-equipped medical laboratories. However, in expanding Point-of-Care (POC) applications (Tüdös et al. 2001; Arora et al. 2010), there is an urgent need for simple and low-cost automated systems capable of performing the plasma separation and mixing operations in a seamless and efficient manner.

Compared to their large-scale counterparts, microfluidic chips have many advantages, including a reduced sample/reagent consumption, a faster response time, a greater throughput, a cheaper cost, greater portability, and so on. The literature contains several proposals for performing continuous real-time blood plasma separation and micromosaic immunoassays (Wolf et al. 2004; Yang et al. 2006). In

J.-N. Kuo (✉) · B.-S. Li
Department of Automation Engineering, National Formosa University, No. 64, Wenhua Rd., Huwei, Yunlin 632, Taiwan
e-mail: junan@nfu.edu.tw

addition, various methods are available for performing blood separation on microfluidic platforms, including specific-to-purpose microchannel structures (Huang et al. 2010), built-in porous filters (Moorthy and Beebe 2003), cross-flow filters (Van Delinder and Groisman 2006; Chen et al. 2007), dielectrophoresis force separation (Huang et al. 2002), and magnetic-activated cell separation (Inglis et al. 2004; Smistrup et al. 2005).

Centrifugal microfluidics, commonly referred to as “Lab-on-CD” (Vilkner et al. 2004; Madou et al. 2006; Li et al. 2009; Gorkin et al. 2010; Mark et al. 2010), is an emerging technology in which a microchip is mounted on the surface of a CD, and the liquid is transported through the chip by means of the centrifugal force generated as the CD rotates. Such devices do not require external pumps to make the fluid flow, and therefore greatly reduce the number of physical connections required to realize the platform. Lab-on-CD devices provide a feasible means of achieving various fluidic functions, including valving (Badr et al. 2002), metering (Andersson et al. 2007), and mixing (Grumann et al. 2005; Ducrée et al. 2005; Nguyen and Wu 2005). Furthermore, CD microfluidic platforms can also be used to achieve blood separation based on the difference in the mass density of the different components of human blood (Haeberle et al. 2006; Zhang et al. 2008) by means of the plasma-skimming effect (Fung 1973) and the centrifugal force induced by CD rotation.

The performance of microfluidic systems is dependent on the rapid and efficient mixing of the sample and reagent. In traditional stationary microfluidic systems, species mixing occurs predominantly as a result of diffusion, and thus an extended mixing time and/or mixing channel is required to achieve a homogenous sample solution (Salmanzadeh et al. 2011). Regarding centrifugal microfluidic platforms, various methods have been proposed for improving the mixing efficiency by means of Coriolis forces (Ducrée et al. 2006), magnetic beads (Grumann et al. 2005; Ducrée et al. 2007), spin direction reversal (Cho et al. 2007), or pneumatic agitation (Kong and Salin 2012). However, these methods generally impose rigid constraints on the required rotational speed and/or direction, or involve a complex fabrication process for both the disk and the centrifugal platform.

Accordingly, the present study proposes a simple Lab-on-CD microfluidic platform for achieving the rapid mixing of reagents and separated blood plasma in a seamless and low-cost manner. In contrast to traditional centrifugal sedimentation methods, in which the blood cells and plasma are separated into different phase layers but are retained in the same reservoir, the proposed platform drives the blood cells and plasma into two separate reservoirs on the disk. As a result, plasma mixing and testing can be performed immediately on the same platform without the need for a further extraction process. The performance of three Lab-on-CD devices incorporating mixing channels with different widths is investigated

both numerically and experimentally. The practical applicability of the proposed device is then demonstrated by performing a PT test (Shih et al. 2012).

2 Experimental design and method

2.1 Plasma separation microchannel network

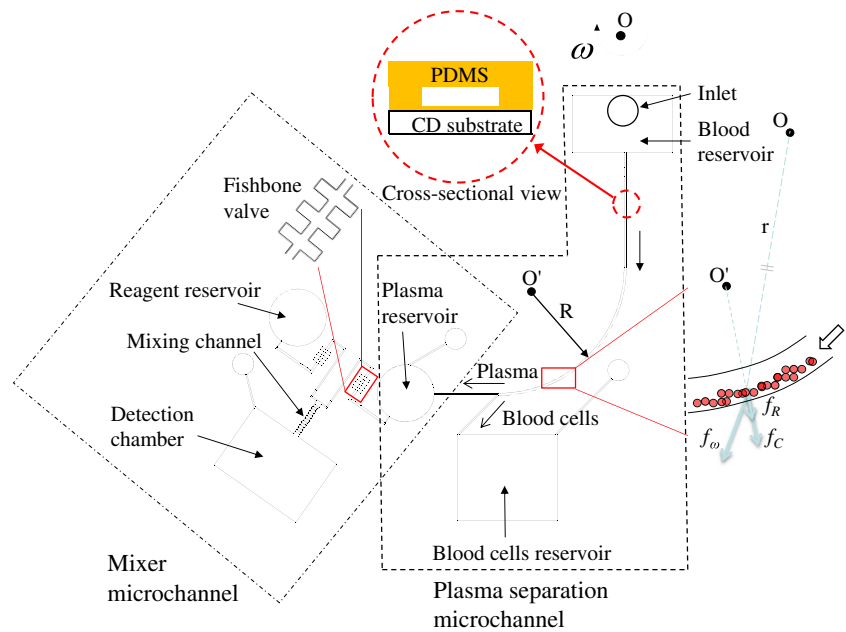
Figure 1 presents a schematic illustration of the proposed CD microfluidic platform. As shown, the device comprises a plasma separation microchannel network and a plasma/reagent mixer network. The plasma separation network consists of a straight microchannel, a curved microchannel and a branched microchannel. In the proposed system, a separation effect is achieved as a result of the difference in density of the blood components (i.e., the plasma and blood cells). As the CD rotates, the blood within the separation network is subjected to three different body forces, namely the centrifugal force f_ω due to system rotation, the Coriolis force f_C due to the combined effects of system rotation and the liquid velocity, and the centrifugal force f_R generated by the microchannel curvature itself. In the straight channel of the separation network, the blood is acted on by the Coriolis force only. However, in the curved region of the network, the blood is subjected to all three body forces, and the blood cells are driven toward the outer wall of the microchannel as a result of their greater density. Thus, on reaching the bifurcation point at the end of the curved microchannel, the blood cells flow into the blood cell reservoir, while the plasma continues in the downstream direction.

In the human blood circulation system, blood cells flowing through a branching blood vessel have a tendency to travel into the wider vessel branch as a result of the higher flow rate (Yang et al. 2006). In the separation network of the microfluidic platform proposed in this study, this so-called Zweifach-Fung effect (Fung 1973) is exploited to further prompt the ingress of the blood cells into the blood cell reservoir by deliberately assigning a greater value to the width of the blood cell channel leading to the blood cell reservoir than that of the plasma channel leading in the downstream direction to the plasma reservoir.

2.2 Mixer microchannel network

As shown in Fig. 1, the plasma mixing microchannel network comprises a plasma reservoir, a reagent reservoir, two fishbone valves, a mixing channel, and a detection chamber. The fishbone valves provide a robust valving function (Lu et al. 2007) and either retain the fluid within the respective reservoir or dispense the fluid into the mixing channel, depending on the CD rotation speed. For the present design, the calculated and experimental values of the burst frequency of

Fig. 1 Schematic illustration of microchannel configuration on CD platform for separation and mixing of blood plasma



the fishbone valves are equal to 2105 rpm and 2140 ± 60 rpm, respectively. In other words, for CD rotation speeds lower than this value, the reagent and blood plasma are retained within their respective reservoirs, while at speeds greater than this value, they are dispensed into the mixing channel.

In a previous study by the present group (Kuo and Jiang 2013), it was shown that a square-wave microchannel yields a better mixing efficiency than a curved microchannel or zigzag microchannel. Thus, in the CD microfluidic chip proposed in the present study, the mixing channel was designed with the square-wave configuration shown in Fig. 2a. In designing the microchannel, the two inlets were assigned a width of $100 \mu\text{m}$, the channel height (H) was set as $400 \mu\text{m}$, the channel depth was specified as $40 \mu\text{m}$, the axial channel length (L) was given as $2350 \mu\text{m}$, the pitch (P) was specified as $350 \mu\text{m}$, and the channel width in the y -axis direction (W_y) was assigned a value of $50 \mu\text{m}$. To determine the optimal mixing performance, the channel width in the x -axis direction (W_x) was assigned three different values, i.e., $50 \mu\text{m}$ (Type 1), $100 \mu\text{m}$ (Type 2) and $150 \mu\text{m}$ (Type 3). As shown in Fig. 2b–d, the mixing channel comprised five periodic units in every case.

2.3 Fabrication process

The CD microfluidic platform was fabricated using conventional soft lithography techniques (McDonald et al. 2002). Briefly, a photomask pattern for each microchannel network was generated using AutoCAD software and was transferred onto a clear transparent film. A photolithography technique was then used to fabricate an SU-8 master of the total microchannel network. The master was then used to transfer

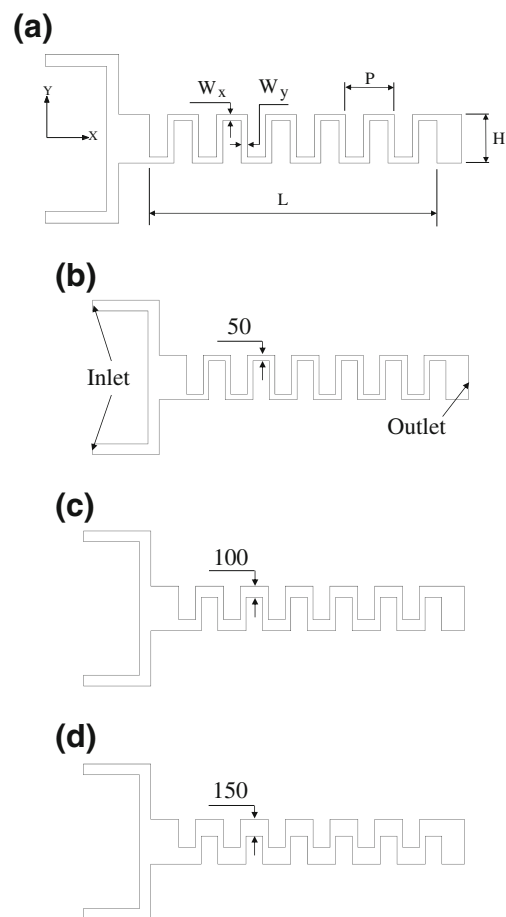


Fig. 2 a Basic geometry parameters of square-wave microchannel. Three mixing channels considered in present study: b Type 1 ($W_x=50 \mu\text{m}$); c Type 2 ($W_x=100 \mu\text{m}$) and d Type 3 ($W_x=150 \mu\text{m}$)

the microchannel network to a poly(dimethylsiloxane) (PDMS) layer with a thickness of 40 μm . A via hole with a diameter of 2 mm was drilled in the inlet reservoir region of the PDMS layer to serve as an inlet for the whole blood sample. The inlet via and the reservoir collectively can hold the blood sample around 10 μL . Meanwhile, three vents (each with a diameter of 1 mm) were drilled in the blood cell, plasma and detection reservoirs/chambers of the microchannel network in order to balance the pressure. The PDMS layer was carefully positioned on a CD (diameter 12.7 cm) and was bonded to the surface by means of an oxygen plasma process involving an initial curing procedure (the PDMS layer with a thickness of 10 μm coated over the CD was performed at a temperature of 70 $^{\circ}\text{C}$ for 3 h), an oxygen plasma treatment process, and a plasma cleaning operation (Harrick, PDC-001).

Referring to Fig. 1, the whole blood reservoir had dimensions of 7 mm \times 4 mm, the blood cell reservoir measured 7 mm \times 6 mm, and the plasma reservoir had a diameter of 4 mm (giving a volume of 0.5 μL). The straight microchannel in the separation network had a length of 8 mm and the curved channel had a radius of 9 mm. Both channels had a width of 160 μm . To induce the Zweifach-Fung effect at the bifurcation point of the branched microchannel, the width of the channel leading to the blood cell reservoir was set as 100 μm , while that of the channel leading to the plasma reservoir was set as 60 μm . In the mixer microchannel network, the reagent reservoir had a diameter of 4 mm and the detection chamber measured 7 mm \times 5 mm. The dimensions of the square-wave mixing channel were set as described in Section 2.2. The channels leading from the plasma and reagent reservoirs to the fishbone valves each had a width of 150 μm . The fishbone valves comprised three parallel microchannels with a length and width of 200 μm and a separation distance of 250 μm . Note that all of the microchannels, valves and reservoirs on the CD microfluidic platform had a depth of 40 μm .

2.4 Experimental setup

The whole human blood was drawn from a healthy male donor and pretreated with the anticoagulant ethylenediaminetetraacetic acid (EDTA). The blood was then diluted with phosphate buffer saline (PBS) to a designated hematocrit concentration level in the range of 6~48 %. The hematocrit is the volume percentage of red blood cells in human blood and is generally around 41~53 % for males. 1.5 μL of human blood and 0.5 μL of de-ionized (DI) water were introduced into the blood inlet reservoir and reagent reservoir, respectively, using a pipette. The CD microfluidic platform was then placed on a spin processor (SP-M2-P, APISC) to perform the plasma separation and mixing process. As discussed in Section 2.2, the burst frequency of the fishbone valves was around 2140 \pm 60 rpm. Thus, in performing the separation process, the CD rotation speed was specified as 2000 rpm,

while in performing the mixing process, the CD rotation speed was set as 2200 rpm. The efficiency of the plasma separation process was evaluated in accordance with (Zhang et al. 2008)

$$\eta = (C_{FC} - C_{PC}) / C_{FC}, \quad (1)$$

where C_{FC} is the cell concentration in the blood inlet reservoir and C_{PC} is the cell concentration in the plasma reservoir. (In both cases, the cell concentration was determined by cell counting.)

The mixing efficiency of microfluidic devices is generally evaluated by examining the concentration distribution of fluorescent dyes or color dyes within the microchannel (Yang et al. 2009). In the present study, the blood plasma was almost completely clear, and thus a small amount of red dye was added to the plasma reservoir in order to increase the contrast between the plasma and the reagent (DI water). The mixing effect during disk rotation was observed using an image acquisition system comprising a stroboscope (DT-311 N, SHIMPO), a triggering sensor, and a high-speed charge-coupled device (CCD) camera (EO-0413C, Edmund Optics). In performing the separation and mixing experiments, the sensor synchronized the stroboscope with the disk rotation speed by detecting the signals reflected from a trigger mark located on the surface of the disk. The captured images were analyzed using digital image processing software in order to evaluate the flow fields and mixing efficiency within the mixing channel. The mixing efficiency of the three square-wave mixing channels was evaluated as (Lu et al. 2002)

$$\sigma = \left\{ 1 - \sqrt{\frac{1}{N} \sum_{i=1}^N \left(\frac{c_i - \bar{c}}{\bar{c}} \right)^2} \right\} \times 100\%, \quad (2)$$

where c_i is the color index of pixel i and \bar{c} is the average color index over N pixels located along a designated sampling line or over a designated sampling area. Note that N was specified as 150 in the present study. Accordingly, we can compare mixing indexes in the channel flow at different cross sections and calculate the mixing time required in a stirred chamber. In Eq. (2), a value of $\sigma=0$ indicates a completely unmixed state of the DI water and blood plasma, while a value of $\sigma=1$ indicates a completely mixed state.

3 Numerical simulations

The separation of the plasma and blood cells in the separation microchannel network was simulated using the particle tracing module of COMSOL (a commercial computational fluid dynamics (CFD) software package). (Full details of the particle tracing module are available in the COMSOL user manual.) In performing the simulations, the hydrostatic pressure in

the inlet blood reservoir due to rotation was taken into account. In addition, the blood flow was assumed to consist of just two phases, namely plasma and red blood cells. The blood cells were assumed to have the form of spherical particles with a diameter of 8 μm and a constant mass.

Numerical simulations were also performed to investigate the mixing performance of the three square-wave mixing channels. As described in Section 2.1, the rotation of the CD generates three body forces within the microchannels on the rotating platform, namely a centrifugal force f_ω , a Coriolis force f_C , and a second centrifugal force f_R . The Coriolis force is an apparent deflective force acting on a moving object being observed from a rotating platform. The magnitude of the Coriolis force is proportional to the speed of the object (liquid) and acts in a direction perpendicular to the direction of motion. The second centrifugal force is an apparent force which draws a moving object away from the center of curvature of the microchannel on a rotating platform. The three forces can be expressed mathematically as follows (Zhang et al. 2008):

$$f_\omega = r\rho\omega^2, \tag{3}$$

$$f_C = 2\rho\omega u, \tag{4}$$

$$f_R = \rho u^2/R, \tag{5}$$

where r is the distance from the rotation center to the point of interest, ρ is the density of the fluid, ω is the angular rotation speed, u is the liquid velocity, and R is the radius of curvature of the microchannel. In simulating the fluid behavior within the three mixing channels, the flow field was estimated by solving the Navier–Stokes equations, while the plasma concentration distribution was calculated by solving the combined convection and diffusion equations. Finally, transient analyses were carried out using fixed-pressure boundary conditions at the inlet and outlet channels and a no-slip boundary condition on the channel walls. The governing equations were specified as follows:

$$\nabla \cdot \mathbf{V} = 0, \tag{6}$$

$$\rho \left[\frac{\partial \mathbf{V}}{\partial t} + (\mathbf{V} \cdot \nabla) \mathbf{V} \right] = \mathbf{F} - \nabla p + \mu \nabla^2 \mathbf{V}, \tag{7}$$

$$\mathbf{F} = \rho \mathbf{g} + \mathbf{F}_{ce} + \mathbf{F}_{co} = \rho \left(\mathbf{g} + \mathbf{r}|\boldsymbol{\omega}|^2 - 2\boldsymbol{\omega} \times \mathbf{V} \right), \tag{8}$$

where \mathbf{V} is the velocity vector, \mathbf{g} is the gravity vector, \mathbf{r} is the radial position vector, and $\boldsymbol{\omega}$ is the angular velocity vector.

In performing the simulations, it was assumed that the mixing process took place under room temperature condition. The density and viscosity of the DI water were thus specified as 997 kg/m³ and 0.9 × 10⁻³ Ns/m², respectively; while the

density and viscosity of the plasma were specified as 1025 kg/m³ and 1.3 × 10⁻³ Ns/m², respectively. Finally, the diffusivities of the DI water and plasma were both set as 1.2 × 10⁻⁹ m²/s (Liu et al. 1997; Hossian et al. 2009).

4 Results and discussion

4.1 Separation results

Figure 3a presents the simulation results for the trajectories of the red blood cells during the plasma separation process. The results confirm that the body forces acting on the whole blood sample cause the blood cells to move toward the outside of the microchannel as a result of their greater density. Moreover, as the blood cells arrive at the bifurcation point, they are drawn into the blood cell reservoir as a result of both the three body forces and the Zweifach-Fung effect, while the plasma continues in the downstream direction toward the plasma reservoir. As described above, the centrifugal force f_ω , Coriolis force f_C and second centrifugal force f_R exert a combined effect in separating the red blood cells from the plasma in the curved region of the microchannel prior to the bifurcation point. In practice the relative contribution of each body force depends on the geometrical parameters of the microchannel. For the CD device fabricated in the present study, the simulation results showed that the three forces were of roughly the same order of magnitude. Moreover, it was found that the three forces were ordered as $f_\omega > f_C > f_R$ in terms of their separation effect at the middle of the curved microchannel given a CD rotation speed of 2000 rpm and a liquid velocity of 5.8 mm/s.

The plasma separation performance of the microfluidic platform was evaluated experimentally using a 1.5 μL diluted whole blood sample with a hematocrit concentration of 6 %. The results showed that the plasma separation process was completed within 5~6 s given a CD rotation speed of 2000 rpm. Figure 3b–d present experimental images of the separation process. As shown in Fig. 3b, the blood cells flow along the outside wall of the curved microchannel and enter the blood cell reservoir after passing the bifurcation point (see Fig. 3c). By contrast, the blood plasma continues in the downward direction once it passes the bifurcation point, and subsequently enters the plasma reservoir (see Fig. 3d). A close examination of Fig. 3b and d shows that very few blood cells remain within the plasma as it flows past the bifurcation point and enters the plasma reservoir. Thus, the effectiveness of the proposed curved microchannel design (and to a lesser extent, the Zweifach-Fung effect) in producing a thorough separation of the blood plasma from the blood cells is confirmed.

Figure 3e shows the separation efficiency of the proposed microfluidic platform for hematocrit concentrations in the range of 6~48 %. From inspection, the separation efficiency

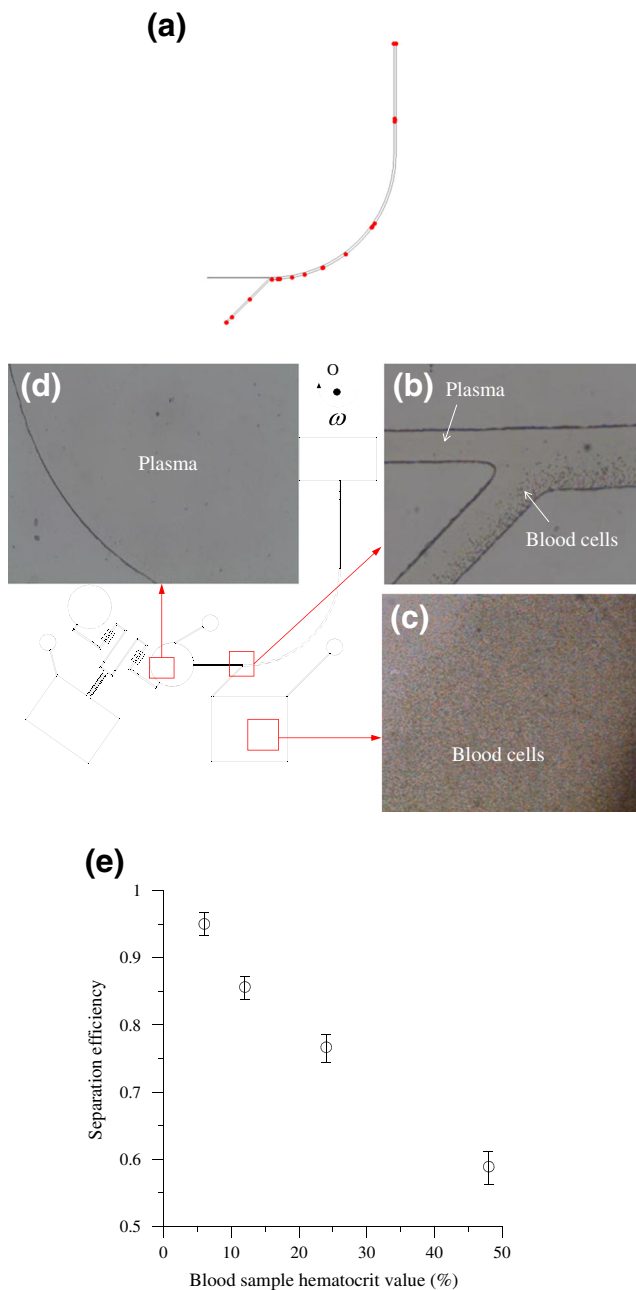


Fig. 3 **a** Simulation results for red blood cell trajectories in plasma separation microchannel network given CD rotation speed of 2000 rpm. Experimental observations of blood plasma separation process: **b** separation of blood cells and plasma at bifurcation point; **c** collection of red blood cells in blood cell reservoir, **d** collection of nearly pure plasma in plasma reservoir, and **e** variation of plasma separation efficiency with hematocrit concentration

for a blood sample with a hematocrit concentration of 6 % is found to be 95 %. It is noted that this value is greater than that of 90 % reported by Blattert (Blattert et al. 2005) for a blood sample with a 5 % hematocrit concentration. However, it should be noted that the efficiency of the device proposed by Blattert can be increased to 95 % given a higher feed velocity. In practice, the superior separation performance of

the proposed device arises due to the combined effects of the three different separation mechanisms (i.e., body forces). In addition, it is noted that while the separation efficiency is less than that of the centrifugal extraction scheme proposed by Haeberle (Haeberle et al. 2006), i.e., 99 %, it is nonetheless adequate for downstream blood PT tests. It is seen in Fig. 3e that the separation efficiency reduces monotonically with an increasing hematocrit concentration. For example, given a hematocrit concentration of 12 %, the separation efficiency reduces to 86 %, while for a hematocrit concentration of 48 % (whole blood), the separation efficiency is just 59 %. The reduction in the separation performance with an increasing hematocrit concentration is to be expected since the intensity of the interactions among the blood cells strengthens as the number of cells increases. Moreover, given a lower hematocrit concentration, the blood has a lower viscosity and therefore flows faster. As a result, both the Coriolis force f_C and the second centrifugal force f_R are increased. It should be noted, however, that a number of other factors may also affect the separation efficiency, such as the temperature, the smoothness and the hydrophilicity of the channel surface, and so on.

4.2 Mixing results

As discussed in Section 3, the mixing performance of the three different square-wave microchannels was evaluated as a function of the CD rotation speed by means of COMSOL simulations. In performing the simulations, the inlet of the mixer was assumed to be located at a radial distance of 45 mm from the center of the CD. Moreover, the two fluids (DI water and plasma) were assumed to enter the microchannel in a laminar condition. Figure 4a shows the plasma concentration distributions within the three microchannels given a CD rotation speed of 2200 rpm and a mixing time of 5 s. (The plasma is indicated in red, while the DI water is shown in blue.) It is seen that for all three channels, the species mixing efficiency increases steadily along the length of the channel. Due to the geometrical shape at the corner, the contact interface between the two fluid streams is located close to the inner wall prior to each 90° turn in the microchannel, but close to the outer wall following each turn. Thus, in passing through each turn, the flow near the inner corner accelerates, while that near the outer corner decelerates. To satisfy the requirement for mass conservation, a vortex structure is therefore formed in each turn of the microchannel. The vortex structures perturb the two species flows; thereby increasing the contact area between them and improving the mixing performance as a result (Hossian et al. 2009). The mixing performance within the square-wave microchannel is further enhanced by the transverse secondary flows along the microchannel induced by the centrifugal and Coriolis forces as well as the stirring effect at the corner (La et al. 2013).

Fig. 4 **a** Plasma concentration distribution in three square-wave microchannels given CD rotation speed of 2200 rpm and mixing time of 5 s. **b** Variation of mixing index at microchannel exit with CD rotation speed for three microchannel designs. **c** Variation over time of mixing index at microchannel exit given CD rotation speed of 2200 rpm and three microchannel designs

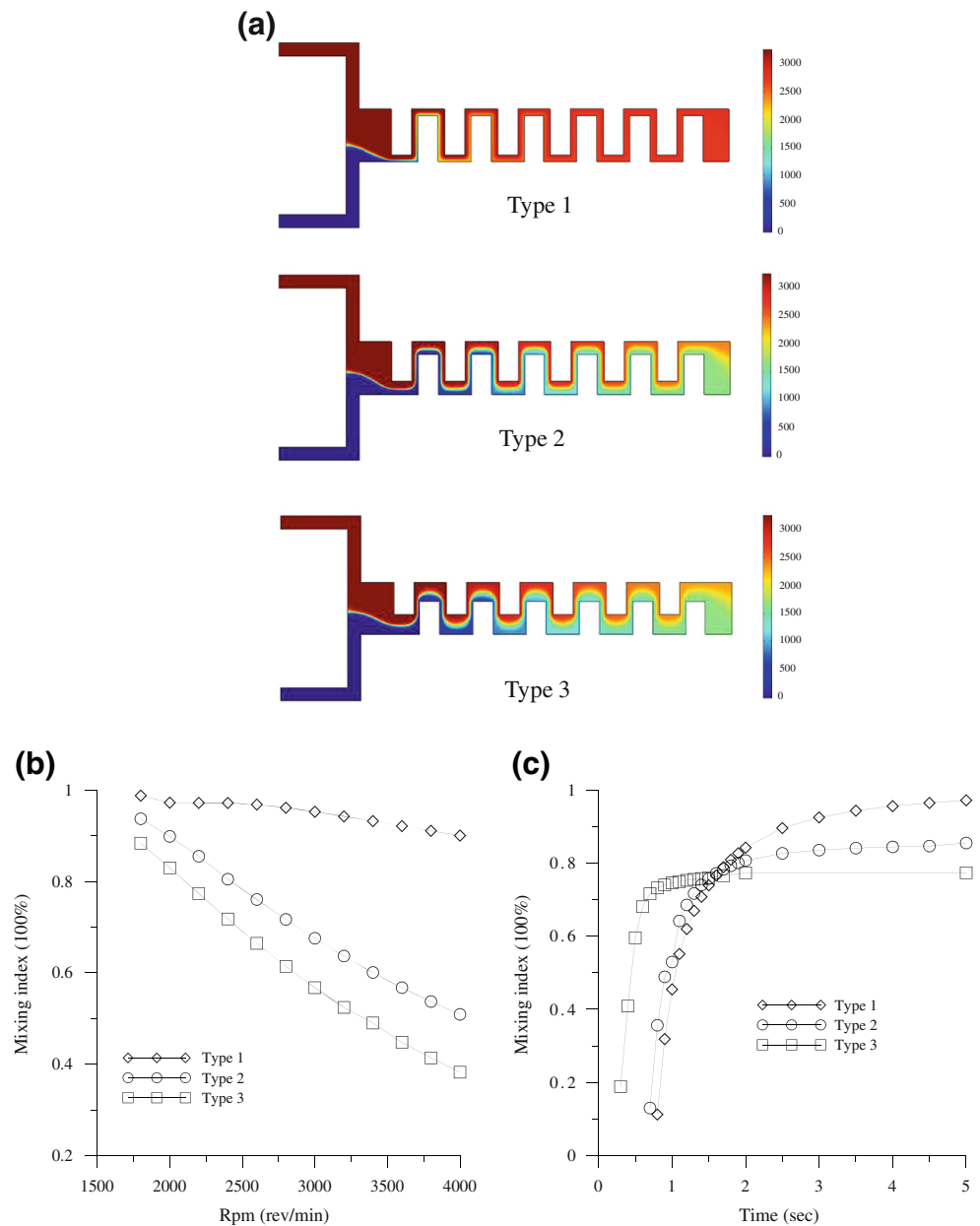


Figure 4b presents the simulation results obtained for the variation of the mixing index at the exit of the three microchannels given CD rotation speeds ranging from 1800 rpm to 4000 rpm. For all three microchannels, the mixing index reduces with an increasing rotation speed due to the corresponding reduction in the residence time. For example, given a rotation speed of 1800 rpm, the residence time within the Type 3 microchannel is equal to 0.55 s, whereas for a rotation speed of 4000 rpm, the residence time is just 0.15 s. Moreover, for a given rotation speed, the optimal mixing performance is obtained in the Type 1 microchannel since the narrower width of the channel results in a stronger eddy-induced chaotic mixing effect at each bend in the channel.

As discussed in Section 4.1, the CD rotation speed was specified as 2000 rpm when performing the separation process. Given this rotation speed, the plasma within the whole blood sample was separated from the cells within 5~6 s. The separation performance was also evaluated at higher rotation speeds of up to 2150 rpm. However, no noticeable increase in the separation efficiency was observed. Thus, the CD rotation speed was set as 2000 rpm in all of the following plasma separation tests. By contrast, in the mixing process, the CD rotation speed was set as 2200 rpm in order to break through the burst frequency of the fishbone valves and achieve a higher mixing performance.

Figure 4c shows the variation over time of the mixing index at the exit of the three microchannels given a constant CD

rotation speed of 2200 rpm. It is observed that the mixing efficiency increases rapidly in all three microchannels. From inspection, the maximum mixing performance in the Type 2 and Type 3 microchannels is found to be 83 % and 78 % after approximately 3 s and 2 s, respectively. The Type 1 microchannel results in the highest mixing performance of the three channels (97 %), but requires a slightly longer mixing time (5 s). It is noted that while this mixing time is the longest of the three channels, it is nevertheless acceptable for most microfluidic applications.

The simulation results for the mixing performance of the three microchannels were validated by means of experimental trials. In each experiment, 0.5 μL of DI water was placed in the reagent reservoir using a pipette, while $\sim 0.5 \mu\text{L}$ of plasma was deposited in the plasma reservoir by means of a blood separation process. Figure 5a–d present experimental images showing the mixing of the two species within the Type 1 microchannel following 0, 0.5, 2.5 and 5 s, respectively. Figure 5a shows that in the stationary condition, the fluids in the two reservoirs are stagnant and no mixing occurs. However, as the CD starts to rotate, the two fluids burst through the fishbone valves and enter the mixing channel, as shown in Fig. 5b. As further time elapses, the two fluids mix within the square-wave microchannel (see Fig. 5c) and subsequently flow into the detection chamber (see Fig. 5d). Applying the formula given in Eq. (2) to the experimental image shown in Fig. 5d, the mixing efficiency is found to be 96 %. Figure 5e presents experimental images of the detection chambers in the CD microfluidic platforms containing the Type 2 and Type 3 mixing channels, respectively, after 5 s. The corresponding mixing efficiencies are equal to 84 % and 76 %, respectively. It is noted that the experimental results for the mixing efficiency are consistent with the simulation results presented in Fig. 4c.

Figure 5f compares the experimental and simulation results for the variation over time of the mixing efficiency of the Type 1 microchannel. It is noted that while the numerical results for the mixing index are slightly higher than the experimental values for the first 3 s (approximately), the simulation results converge to the experimental values after 5 s. Thus, the validity of the numerical simulation results is confirmed.

4.3 Prothrombin time test

The practical feasibility of the proposed CD microfluidic platform was investigated by performing a PT test. PT tests are widely used in clinical practice to measure the time required for blood to coagulate and to determine an appropriate drug dose for patients undergoing oral anti-coagulation therapy. In clinical practice, PT tests are usually performed using plasma samples without a blood cell concentration. The reference range for a plasma PT test depends on the analytical method used, but is usually around 10–15 s. Figure 6a

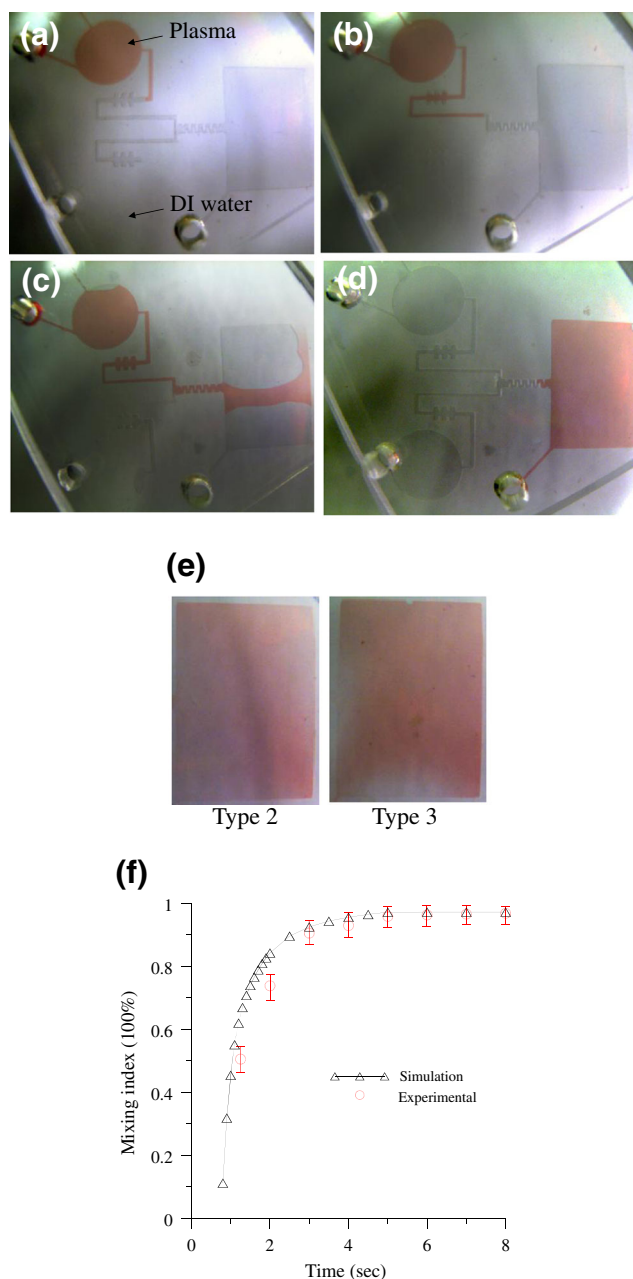


Fig. 5 Experimental images showing mixing of blood plasma and DI water in Type 1 microchannel after: **a** 0 s; **b** 0.5 s; **c** 2.5 s; **d** 5 s; and in **e** detection chambers in CD microfluidic platforms incorporating Type 2 and Type 3 microchannels after 5 s. **f** Comparison of simulation and experimental results for variation of mixing index of Type 1 microchannel over time. Note that the CD rotation speed is 2200 rpm

presents a schematic illustration of the experimental setup used to perform the PT test in the present study. The optical detection system comprised a 10 mW diode laser with a central wavelength of 405 nm (SDL-405-LM-010 T, Shanghai Dream Lasers), a variable ND filter in order to control the optical intensity of the output beam, and a spectrometer (USB2000+, Ocean Optics) to measure the intensity of the transmitted light. The data acquired by the spectrometer

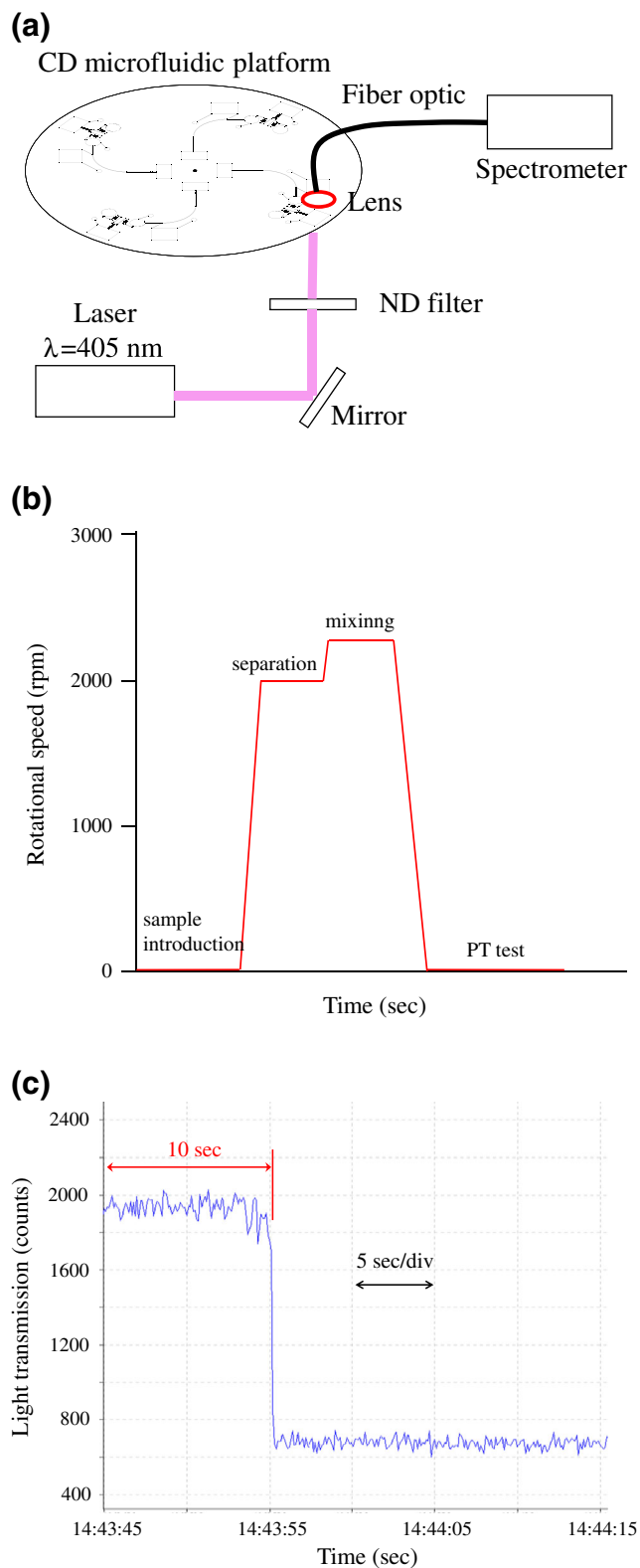


Fig. 6 **a** Schematic illustration of experimental setup used to perform PT test. **b** Timeline for PT test. **c** Intensity of transmitted light recorded by spectrometer during PT test

were recorded using SpectraSuite software (SpectraSuite Version 5.1, Ocean Optics).

In performing the PT test, $1.5 \mu\text{L}$ of blood was injected into the inlet blood reservoir and $0.5 \mu\text{L}$ of PT reagent (Dade[®] Innovin[®]) was placed in the reagent reservoir. The CD was then rotated at 2000 rpm for 5 s in order to deposit $\sim 0.5 \mu\text{L}$ of plasma in the plasma reservoir. The rotation speed was then increased to 2200 rpm for a further 5 s in order to produce a mixed flow of plasma and PT reagent into the detection chamber. Following the mixing process, the CD was rotated manually such that the detection chamber was illuminated by the laser beam emerging from the ND filter. Figure 6b presents the timeline for the entire PT test. The time required to form fibrin clots as a result of the coagulation process between the plasma and PT reagent was measured optically by the spectrometer. Figure 6c shows the PT measurement curve for a whole blood sample with a hematocrit concentration of 48 %, in which the x-axis shows the time and the y-axis shows the light transmission amplitude. After the mixing process, the residual blood cells fall to the bottom of the detection chamber as a result of their greater density. Thus, in obtaining the results presented in Fig. 6c, the laser beam was aimed at the top of the detection chamber in order to exclude the effects of these blood cells when determining the coagulation time. It is seen that the amplitude of the transmitted light has a high and constant value for the first 10 s of the detection period. Thus, it is inferred that very little fibrin is formed. However, after 10 s, the intensity of the transmitted light reduces sharply and remains approximately constant as further time elapses, indicating the completion of the coagulation process. The total time of the PT test, including the sample/reagent injection time, the blood separation time, the plasma mixing time and the coagulation time was found to be less than 1 min. This time is significantly less than that of a typical PT test bench top system (Sysmex CA1500 coagulation analyzer), i.e., around 15 min (Shih et al. 2012).

The PT test was repeated using blood samples with various hematocrit concentrations in the range of 6–24 %. The results showed that the coagulation time increased with a decreasing hematocrit concentration. For example, the coagulation time for a sample with a 24 % hematocrit concentration was found to be 25 s, while for samples with hematocrit concentrations of 12 % and 6 %, the coagulation time was found to be 40 s and 70 s, respectively. The lengthening of the coagulation time with a decreasing hematocrit concentration is to be expected since the interactions among the fibrins are weakened as the hematocrit concentration reduces.

5 Conclusions

This study has presented a lab-on-CD microfluidic platform for the rapid separation and mixing of blood plasma. The performance of the proposed device has been evaluated both numerically and experimentally. The experimental results

have shown that a plasma separation efficiency of up to 95 % can be achieved within 5~6 s for a diluted blood sample with a hematocrit concentration of 6 %. Moreover, it has been shown that the separation efficiency increases monotonically as the hematocrit concentration decreases. The mixing performance of three square-wave microchannels with different widths has been analyzed and compared. The results have shown that the mixing efficiency improves as the channel width is reduced. Given a CD rotation speed of 2200 rpm and a channel width of 50 μm , a mixing efficiency of 96 % can be obtained within 5 s. The feasibility of the proposed CD platform for clinical applications has been demonstrated by performing a PT test. It has been shown that the test can be accomplished using a total sample volume (blood and reagent) of just 2 μL . Moreover, the test can be completed within 1 min rather than the 15 min required by a typical bench top system. The CD microfluidic platform proposed in this study has many practical advantages compared to existing devices, including a low cost, a straight-forward fabrication process, a low sample/reagent consumption, and a high portability. As a consequence, it provides an ideal solution for Point-of-Care (POC) clinical diagnostic applications.

Acknowledgments The authors gratefully acknowledge the financial support provided to this study by the National Science Council of Taiwan under Grant No. NSC 101-2221-E-150-036. In addition, the access provided to fabrication equipment by the Common Lab for Micro/Nano Science and Technology of National Formosa University is also greatly appreciated.

References

- P. Andersson, G. Jesson, G. Kylberg, G. Ekstrand, G. Thorsén, *Anal. Chem.* **79**(11), 4022 (2007)
- A. Arora, G. Simone, G.B. Salieb-Beugelaar, J.T. Kim, A. Manz, *Anal. Chem.* **82**(12), 4830 (2010)
- I.H.A. Badr, R.D. Johnson, M.J. Madou, L.G. Bachas, *Anal. Chem.* **74**(21), 5569 (2002)
- C. Blattert, R. Jurischka, A. Schoth, P. Kerth, W. Menz, *Proc. SPIE* **5651**, 196 (2005)
- X. Chen, D.F. Cui, C.C. Liu, H. Li, *Sensors Actuators B* **130**, 216 (2007)
- Y.K. Cho, J.G. Lee, J.M. Park, B.S. Lee, Y.S. Lee, C. Ko, *Lab Chip* **7**, 565 (2007)
- J. Ducreé, S. Haerberle, T. Brenner, T. Glatzel, R. Zengerle, *Microfluid. Nanofluid.* **2**, 97 (2005)
- J. Ducreé, T. Brenner, S. Haerberle, T. Glatzel, R. Zengerle, *Microfluid. Nanofluid.* **2**, 78 (2006)
- J. Ducreé, S. Haerberle, S. Lutz, S. Pausch, F.V. Stetten, R. Zengerle, *J. Micromech. Microeng.* **17**(7), S103 (2007)
- Y.C. Fung, *Microvasc. Res.* **5**(1), 34 (1973)
- R. Gorkin, J. Park, J. Siegrist, M. Amasia, B.S. Lee, J.M. Park, J. Kim, H. Kim, M. Madou, Y.K. Cho, *Lab Chip* **10**(14), 1758 (2010)
- M. Grumann, A. Geipel, L. Riegger, R. Zengerle, J. Ducreé, *Lab Chip* **5**(5), 560 (2005)
- S. Haerberle, T. Brenner, R. Zengerle, J. Ducreé, *Lab Chip* **6**, 776 (2006)
- S. Hossian, M.A. Ansari, K.Y. Kim, *Chem. Eng. J.* **150**, 492 (2009)
- Y. Huang, S. Joo, M. Duhon, M. Heller, B. Wallace, X. Xu, *Anal. Chem.* **74**, 3362 (2002)
- C.T. Huang, P.N. Li, C.Y. Pai, T.S. Leu, C.P. Jen, *Sep. Sci. Technol.* **45**, 42 (2010)
- D.W. Inglis, R. Riehn, R.H. Austin, J.C. Sturm, *Appl. Phys. Lett.* **85**, 5093 (2004)
- C.M. Jackson, M.P. Esnouf, *Clin. Chem.* **51**, 483 (2005)
- M.C.R. Kong, E.D. Salin, *Microfluid. Nanofluid.* **13**, 519 (2012)
- J.N. Kuo, L.R. Jiang, *Microsyst. Technol.* **20**(1), 91 (2014)
- M. La, S.J. Park, H.W. Kim, J.J. Park, K.T. Ahn, S.M. Ryew, D.S. Kim, *Microfluid. Nanofluid.* **15**, 87 (2013)
- C. Li, X. Dong, J. Qin, B. Lin, *Anal. Chim. Acta.* **640**, 93 (2009)
- M. Liu, J.K. Nicholson, J.A. Parkinson, J.C. Lindon, *Anal. Chem.* **69**, 1504 (1997)
- L.H. Lu, K.S. Ryu, C. Liu, *J. Microelectromech. Syst.* **11**(5), 462 (2002)
- C. Lu, Y. Xie, Y. Yang, M.M.C. Cheng, C.G. Koh, Y. Bai, L.J. Lee, *Anal. Chem.* **79**, 994 (2007)
- M. Madou, J. Zoval, G. Jia, H. Kido, J. Kim, N. Kim, *Ann. Rev. Biochem. Eng.* **8**, 601 (2006)
- D. Mark, S. Haerberle, G. Roth, F.V. Stetten, R. Zengerle, *Chem. Soc. Rev.* **39**(3), 1153 (2010)
- J.C. McDonald, M.L. Chabiny, S. Metallo, J.R. Anderson, A.D. Stroock, G.M. Whitesides, *Anal. Chem.* **74**, 1537 (2002)
- J. Moorthy, D.J. Beebe, *Lab Chip* **3**, 62 (2003)
- N.T. Nguyen, Z. Wu, *J. Micromech. Microeng.* **15**, R1 (2005)
- A. Salmanzadeh, H. Shafiee, R.V. Davalos, M.A. Stremler, *Electrophoresis* **32**(18), 2569 (2011)
- C.H. Shih, C.H. Lu, J.H. Wu, C.H. Lin, J.M. Wang, C.Y. Lin, *Sensors Actuators B* **161**, 1184 (2012)
- K. Smistrup, O. Hansen, H. Bruus, M.F. Hansen, *J. Magn. Magn. Mater.* **293**, 597 (2005)
- M. Toner, D. Irimia, *Annu. Rev. Biomed. Eng.* **7**, 77 (2005)
- A.J. Tüdös, G.A.J. Besselink, R.B.M. Schasfoort, *Lab Chip* **1**, 83 (2001)
- V. Van Delinder, A. Groisman, *Anal. Chem.* **78**, 3765 (2006)
- T. Vilknér, D. Janasek, A. Manz, *Anal. Chem.* **76**, 3373 (2004)
- M. Wolf, D. Juncker, B. Michel, P. Hunziker, E. Delamarche, *Biosens. Bioelectron.* **19**(10), 1193 (2004)
- S. Yang, A. Undar, J.D. Zahn, *Lab Chip* **6**, 871 (2006)
- S.Y. Yang, J.L. Lin, G.B. Lee, *J. Micromech. Microeng.* **19**(3), 035020 (2009)
- J. Zhang, Q. Guo, M. Liu, J. Yang, *J. Micromech. Microeng.* **18**, 125025 (2008)